International Journal of Biological Macromolecules 253 (2023) 127294

Contents lists available at ScienceDirect

International Journal of Biological Macromolecules

journal homepage: www.elsevier.com/locate/ijbiomac

Microscopy and modelling investigations on the morphology of the biofilm exopolysaccharide produced by *Burkholderia multivorans* strain C1576

Michele Cacioppo [a,1], Rita De Zorzi [a], Zois Syrgiannis [b,c], Barbara Bellich [d,2], Paolo Bertoncin [d], Ining A. Jou [e], John W. Brady [e], Roberto Rizzo [d], Paola Cescutti [d,*]

[a] Department of Chemical and Pharmaceutical Sciences, INSTM UdR Trieste, University of Trieste, Via Licio Giorgieri 1, 34127 Trieste, Italy
[b] Simpson Querrey Institute, Northwestern University, Chicago, IL 60611, USA
[c] Department of Chemistry, Northwestern University, Evanston, IL 60208, USA
[d] Department of Life Sciences, University of Trieste, Via Licio Giorgieri 1, 34127 Trieste, Italy
[e] Food Science Department, Cornell University, 101A Stocking Hall, Ithaca, NY 14853, USA

ARTICLE INFO

Keywords:
Burkholderia multivorans biofilm
Polysaccharide AFM
TEM and modelling
Polysaccharide functions

ABSTRACT

Bacteria form very often biofilms where they embed in a self-synthesized matrix exhibiting a gel-like appearance. Matrices offer several advantages, including defence against external threats and the easiness of intercellular communication. In infections, biofilm formation enhances bacteria resistance against antimicrobials, causing serious clinical problems for patients' treatments. Biofilm matrices are composed of proteins, extracellular DNA, and polysaccharides, the latter being the major responsible for matrix architecture. The repeating unit of the biofilm polysaccharide synthesized by *Burkholderia multivorans* strain C1576 contains two mannoses and two sequentially linked rhamnoses, one of them 50 % methylated on C-3. Rhamnose, a 6-deoxysugar, has lower polarity than other common monosaccharides and its methylation further reduces polarity. This suggests a possible role of this polysaccharide in the biofilm matrix; in fact, computer modelling and atomic force microscopy studies evidenced intra- and inter-molecular non-polar interactions both within polysaccharides and with aliphatic molecules. In this paper, the polysaccharide three-dimensional morphology was investigated using atomic force microscopy in both solid and solution states. Independent evidence of the polymer conformation was obtained by transmission electron microscopy which confirmed the formation of globular compact structures. Finally, data from computer dynamic simulations were used to model the three-dimensional structure.

1. Introduction

Microbial communities often exhibit a collective lifestyle where bacterial cells are embedded in a gel-like matrix [1]. This community is called a "biofilm" and offers several advantages to bacteria, such as protection against many external threats [2], storage of nutrients, and an effective way to communicate through the "quorum sensing system" thanks to cell proximity [3]. The biofilm matrix includes different molecular species biosynthesized by bacteria and excreted into the environment [4]. Among these, polysaccharides, proteins, and nucleic acids, due to their polymeric nature, can form extended hydrated networks embedding bacterial cells [5]. It is generally believed that polysaccharides constitute the main structural component of the biofilm matrix [6]. The architecture of the gel-like matrix is poorly known, but it is clear that it depends on the bacterial species forming the biofilm and the specific biopolymers it synthesizes. This is particularly true for polysaccharides. The investigation of the structure and chemical properties of many polysaccharides extracted from biofilms of different bacterial species [6] led to the identification of very different monosaccharide compositions and sequences, with different chemical-physical properties, suggesting that distinct ways of interaction are responsible for the set-up of the matrix network. In addition, many

* Corresponding author at: Department of Life Sciences, University of Trieste, via L. Giorgieri 1, Bdg C11, 34127 Trieste, Italy.
E-mail address: pcescutti@units.it (P. Cescutti).
[1] Present Address: Department of Biological, Chemical and Pharmaceutical Sciences and Technologies (STEBICEF), University of Palermo, Viale delle Scienze, Ed. 17 - Stanislao Cannizzaro, 90128 Palermo, Italy.
[2] Present address: Department of Advanced Translational Diagnostics, Institute for Maternal and Child Health, IRCCS "Burlo Garofolo", Via dell'Istria 65, 34137 Trieste, Italy.

https://doi.org/10.1016/j.ijbiomac.2023.127294
Received 23 August 2023; Received in revised form 26 September 2023; Accepted 5 October 2023
Available online 7 October 2023

bacterial species can synthesize more than one type of polysaccharide, and clarifying which is the more relevant for the efficient formation of the biofilm matrix is crucial to defining the molecular forces stabilizing it, and eventually to devise possible strategies to disrupt biofilms. As an example, species belonging to the *Burkholderia cepacia* Complex can synthesize at least 10 structurally different polysaccharides but not all of them seem to be involved in stabilizing the biofilm matrix [7]. In addition, alginate, which is produced by the well-investigated *Pseudomonas aeruginosa*, was long believed to be the polymer mainly responsible for biofilm matrix formation, but further studies demonstrated that other polysaccharides (Ps1 and Pel) might play a more crucial role in biofilm formation, while alginate is not necessarily required [8]. Finally, it is worth mentioning that the strain H111 of *Burkholderia cenocepacia* produces two significantly different polysaccharides, one water-insoluble, while the second is fully soluble [9,10]. Their different chemical behaviour strongly suggests that these two polymers have distinct functions in the overall biofilm matrix architecture formation and maintenance.

For the last twenty years, our laboratory has been structurally investigating polysaccharides synthesized by components of the *Burkholderia cepacia* Complex, both in non-biofilm and in biofilm formation conditions. The *B. cepacia* Complex is a family of at least 22 genetically closely related bacterial species [11–14]. Many of them are opportunistic bacteria causing serious, and sometimes lethal, infections in cystic fibrosis or immunodepressed patients [15]. Recently, the investigation of one of the components of the Complex, *B. multivorans* strain C1576, led us to determine the structure of a polysaccharide exhibiting an interesting repeating unit of four monosaccharides, two mannoses and two rhamnoses, with a specific pattern: the two rhamnose (Rha) units are sequentially linked and methylation in position 3 on one of them occurs in 50 % of the repetitive units [16]. Rha is a 6-deoxysugar, with lower polarity than other common monosaccharides. The methylated Rha, 25 % of all Rha sugars of this polysaccharide, has a polarity further reduced. We investigated the polysaccharide extracted from biofilms formed by the *B. multivorans* C1576 strain, hereafter referred to as polysaccharide EpolC1576, to establish whether the low polarity of its primary structure has some role in biofilm matrix setup and function. While biofilm matrices are highly hydrated systems, their gel-like appearance implies that their polymeric skeletons have some degree of insolubility in water.

Previous investigations were able to assess that the Epol C1576 polysaccharide backbone is able to form non-polar interactions with small aliphatic species mimicking components of the quorum system and, thus, suggesting a possible model for transport of molecules with low water solubility through the matrix between bacterial cells [17]. A more recent investigation, carried out by atomic force microscopy (AFM) in the dry state, was able to assess the morphology of the EpolC1576 chain, showing that the polymer adopts a globular structure and, under suitable concentration conditions, assembles to form large aggregates [18]. In the present paper, we discuss new data obtained on EpolC1576 by atomic force microscopy both in the dry state and in solution at a lower concentration, to further clarify the structure-function relationship of this polysaccharide. In addition, AFM data are compared with independent structural data obtained by transmission electron microscopy (TEM). Finally, molecular dynamics calculations have been carried out to parallel the experimental structural findings with reliable models of the polysaccharide three-dimensional conformation.

2. Experimental

2.1. Bacterial strain and Epol C1576 production and purification

Burkholderia multivorans strain C1576 (LMG 16660) is a reference strain from the panel of *Burkholderia cepacia* Complex strains [19] and was purchased from BCCM™bacteria collection (Dept. of Biochemistry and Microbiology, Faculty of Sciences of Ghent University, Belgium). Bacteria growth and polysaccharide purification were performed according to Protocol II described in Ref. [16]. A ^{1}H NMR spectrum of the purified Epol C1576 was recorded to check its purity.

High-performance size exclusion chromatography (HP-SEC) analysis of the exopolysaccharide was performed on an Agilent Technologies 1200 series HPLC equipped with three TSK gel columns (Tosoh Bioscience) in series: G3000PW (<50,000 Da), G5000PW (<1×10^6 Da) and G6000PW (<8×10^6 Da), with internal diameter of 7.5 mm, length of 30 cm and kept at 40 °C in a thermostat-controlled column compartment (Agilent Technologies). Calibration of the chromatographic system was done using pullulan standards (Polymer Laboratories, Germany; Sigma, Germany, for pullulan with molecular mass = 1.6 × 106). Elution was performed with 0.15 M NaCl, using a flow rate of 0.5 mL/min, and monitored using a refractive index detector (Knauer, Labservice Analytica), interfaced with a computer via Agilent software.

2.2. Atomic force microscopy

For AFM experiments in the dry state, samples were prepared by spray-drying diluted and pre-filtered (Millipore 0.22 μm pore-size membranes) polysaccharide solutions (0.05, 0.5, and 5 μg/mL) on freshly cleaved mica surface. Solutions were sprayed using a commercial airbrush (ABEST AB138 kit) previously washed with water and absolute ethanol. The sprayed samples were dried in open air at room temperature for 48 h. Images were acquired on a Multimode™ AFM (Veeco metrology) equipped with a HQ:NSC19/AL_BS tip (MikroMasch, radius 8 nm), using a Nanoscope IIIa controller (Veeco metrology). The images were acquired with 150–275 kHz drive frequency and 250–300 mV drive amplitude and subsequently analysed using Gwyddion v2.50 software.

Following standard procedures for AFM experiments in the liquid state, polymer samples were prepared as follows: a drop of the polysaccharide solution (1 mM, 10 μL) was transferred on a freshly cleaved mica surface, subsequently diluted with 150 mM NaCl solution (2 times), followed by the addition of 20 mM $CaCl_2$ solution used for stabilizing macromolecules on the mica. The total amount of liquid on mica was about 100 μL which is needed to cover the cantilever. AFM images were captured in PeakForce tapping mode on a Dimension Icon AFM (Bruker) with a silicon nitride cantilever (SNL10-A, Bruker) in a liquid cell (Dimension FastScan® Atomic Force Microscope).

2.3. Transmission electron microscopy

Samples were dispersed on a 200-mesh copper grid (Electron Microscopy Sciences), previously prepared with a layer of carbon, and stained with uranyl acetate (saturated solution) following two different deposition methods. (a) Fast-drying procedure: a 4 μL drop of a 10 μg/mL solution of Epol C1576 in water was deposited on an uncharged grid and a 2–3 μL drop of uranyl acetate solution was added on top of the sample. After 1-min incubation, the solution was dried with filter paper (Whatman, grade 1) from the edge of the grid. A 2 μL drop of stain was added to the grid and quickly blotted from the edge. The staining procedure was repeated twice. (b) Slow-drying procedure: a 4 μL drop of 5 μg/mL solution of Epol C1576 was deposited on an uncharged grid and allowed to dry overnight. The following day a drop of uranyl acetate solution (3 μL) was deposited on the grid, incubated for 30 s, and dried with filter paper from the edge of the grid. The staining procedure was repeated twice. Grids were analysed on a Philips EM208 Transmission Electron Microscope (TEM) operating at 100 kV and images were acquired on a Quemesa camera (Olympus Soft Imaging Solutions), using the RADIUS software.

2.4. Chain folding modelling

2.4.1. Single long polysaccharide in vacuum

The first set of simulations was performed with a long polysaccharide

of 34 repeat units, for a total of 136 monosaccharides in the chain. The polysaccharide was configured into a large loose coil as shown in Fig. 6 (left). The system was then minimized, heated to 300 K, then simulated in vacuum for 500 ns using the Langevin dynamics algorithm in the CHARMM molecular mechanics program [20,21], with a step size of 2 fs to gauge the dynamic flexibility of the chains. All simulation parameters were the same as in our previous work [22].

2.4.2. Multiple short polysaccharides in solution

A simulation using independent chains in an aqueous solution was conducted to assess any tendency of C1576 to self-associate. The simulated system consisted of 16 short C1576 polysaccharide chains. Each of the polysaccharide strands was four repeat units in length, or 16 monosaccharides, and it was constructed using the disaccharide minimum energy conformational angles calculated in previous work [23]. These initially ideally structured polysaccharides were then placed in a regular lattice with 4 chains identically oriented and placed side-by-side in a plane with approximately 8 Å separation between each chain, and with four such layers in total, with an approximate 8 Å separation between each layer. This lattice was then placed into a previously-equilibrated cubic box of TIP3P [24,25] water molecules, side dimension of 56 Å, removing overlapping water molecules, yielding a system with 4468 water molecules and 16 short polysaccharide chains, and an approximately 50 % polysaccharide-to-water mass ratio. After the system of polysaccharides and water molecules was set up in CHARMM, the actual simulations were transferred to the AMBER molecular dynamics program [26] for better computational efficiency, using the supercomputer COMET [27] in the ACCESS (formerly XSEDE) network. The system was first briefly minimized, heated to 300 K, and then equilibrated for at least 70 ns until the initial ordered state of the polysaccharides was no longer qualitatively discernible. The end-to-end distance was monitored during the equilibration stage, as shown in Supplementary Materials (Supplementary Fig. S1), to verify that the extension of each polysaccharide had come close in range to the end-to-end distance observed subsequently during the production stage. The simulation procedures and conditions have been previously described [23], with the difference that a strong constraining force was applied during the heating and minimization, with a force constant of 300 kcal/mol/rad^2, which was then turned off during the equilibration and production stages of the simulation. This protocol allows the initial equilibration of water molecules around the polysaccharides. Initial velocities were assigned from a Boltzmann distribution and the initial structures were heated from 0 to 300 K over 100 ps, equilibrated for a total of 72 ns, and then simulated for 600 ns using a Leapfrog Verlet integrator, with a step size of 2 fs and a friction coefficient set at 2.0 ps^{-1}. All other simulation parameters were kept as in previous simulations in solution [23].

3. Results and discussion

The primary structure of Epol C1576 has been clarified in a previous paper [16]. The interesting feature of this structure is the presence of a Rha-Rha pair, where one Rha residue exhibits partial *O*-methylation (Scheme 1), producing segments with lower polarity on the polymer backbone.

3.1. AFM investigation

This feature prompted us to search for the effects of this low polarity. It was demonstrated that Epol C1576 is able to bind aromatic molecules [17]. In addition, the aggregation tendency of the polysaccharide was previously demonstrated by atomic force microscopy (AFM) experiments carried out by spray-drying an aqueous solution (30 μg/L) on freshly cleaved mica surfaces [18]. In the present study, we describe further AFM experiments carried out both in solution and in a spray-dried state, where a low percentage of hydration water is expected to be still present around the polymer. Aiming at reducing unwanted effects of sample preparation that could lead to polysaccharide aggregation, these new experiments were carried out using very diluted solutions (from 0.05 to 0.5 and 5.0 μg/mL).

The "dry state" experiments evidenced two distinct morphologies. On one hand, isolated spherical objects were detected when very diluted solutions (0.05 μg/L) were used (Fig. 1, with the relevant profiling data). Objects with different diameters are present, reflecting the molecular mass polydispersity of the polymer. The vertical height of the profiled objects was estimated to be 2–3 nm for the smaller and 7 nm for the larger objects, suggesting that indeed single polymer chains have been spotted. It should be emphasized that horizontal dimensions are not reliable since they are largely affected by the microscope tip dimension, as reported in the literature.

When a higher concentration of the polymer (0.5 or 5 μg/mL) was used to produce the spray-dried samples on mica, more complex objects were detected (Fig. 2). Fig. 2a shows objects with a more structured morphology compared to those exhibited in Fig. 1a, whose profiling (Fig. 2b and c) might suggest the formation of dimers or multimers. Analysis of the profiles (Fig. 2e) yielded an estimation of the vertical size, i.e. perpendicular to the mica surface, ranging from 10 to 30 nm. Assuming a global spherical shape, these values can be correlated to the diameters of the objects and, considering the data obtained using a more dilute solution (Fig. 1), they confirm the possibility of multichain structures, as also indicated by the comparison between the profiling statistics of the objects detected from dilute solutions and those obtained from more concentrated solutions (Supplementary Fig. S2).

The presence of multichain aggregates can also be inferred by the bimodal profile observed in the spray-dried sample (Fig. 2c), suggesting the association of two or more polymer chains. It is worth noticing that all the objects spotted in the image of Fig. 2a exhibit the same morphology indicating a similar aggregation geometry of the polymeric chains. What is more difficult to explain, but might be probably due to an effect of the spray procedure, is the very similar, if not identical, orientation of the aggregates on the mica surface. In conclusion, the data of "dry state" AFM experiments show that at very low concentrations the Epol C1576 assumes a compact globular structure, without any occurrence of a more extended linear configuration. In addition, data confirm that, in more concentrated solutions, multimer aggregates are formed, as previously demonstrated in our laboratories using more concentrated polysaccharide solutions [18].

Data obtained by AFM from the dry-state samples are certainly interesting, shining light on the three-dimensional properties of Epol C1576. However, the drying process could force the polysaccharide to assume overall structures more compact than those it exhibits in the aqueous environment around the bacteria cells or in biofilms produced by this strain. To elucidate the solution behaviour of the polymer, in parallel to "dry state" experiments, we performed "solution state" AFM imaging by depositing thin layers of a polysaccharide aqueous solution on freshly cleaved mica surfaces. The images obtained were of good quality (Fig. 3) and comparison with the spray-dried samples (Fig. 1 and

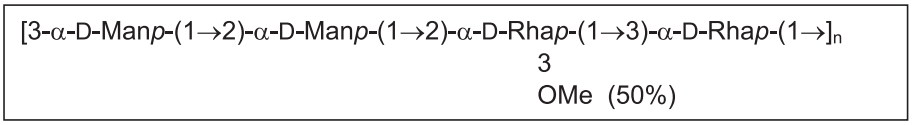

Scheme 1. Structure of the repeating unit of the Epol C1576.

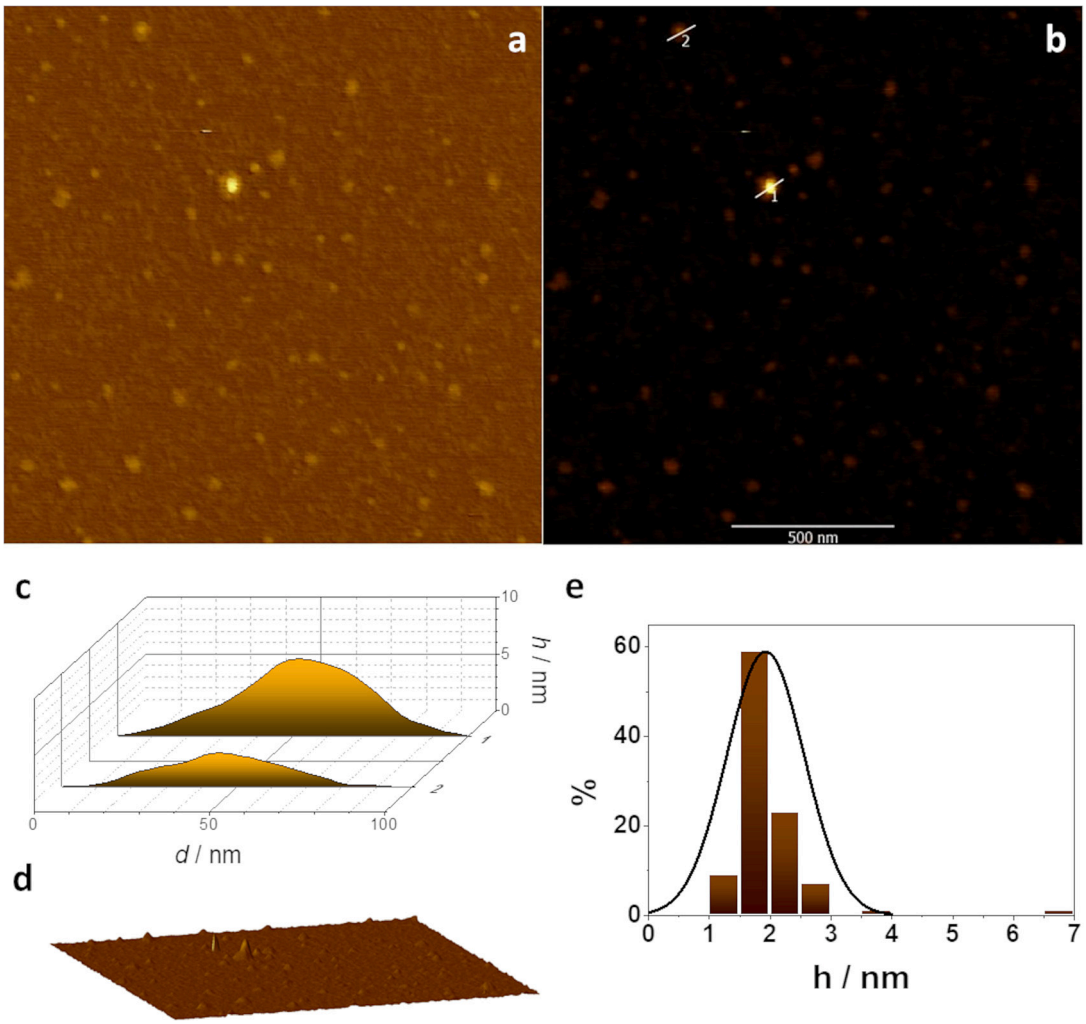

Fig. 1. Dry state AFM image of Epol C1576 taken from a 0.05 μg/mL solution. a) spherical objects present on the mica surface; b) profiling of two of objects exhibiting different dimensions; c) estimation of the vertical dimension of the profiled objects; d) three-dimensional view of panel a); e) statistics of the vertical dimensions of the objects in panel a).

Fig. 2) shows that Epol C1576 in solution maintains a globular conformation with defined morphology. The vertical profiling of the objects indicates the probable presence of molecular multimers but the dimension of the multimer is difficult to assess. As expected, the high hydration level produces a swelling of the globules which leads to larger dimensions compared to the "dry state".

In addition, the striking morphological similarity of "dry" and "solution" states indicates that the polysaccharide maintains the same structure in both states, suggesting that the three-dimensional conformation is very stable. An enlargement of an AFM image reporting a single object from the liquid state is shown in Fig. 3c. The image shows clearly visible details of the morphology of the overall conformation of the polysaccharide in solution. Chain folding was also detected and the same motif is repeated in every object, indicating a similar structural situation. It might be speculated that the low polarity Rha sequences could join together, bringing close to each other sequences of the polymer chain that are topologically distant, or that belong to different chains in a fashion that could recall β-pleated sheets in proteins.

3.2. TEM investigation

To obtain independent information on the polymer chain morphology which Epol C1576 assumes, transmission electron microscopy (TEM) experiments were carried out. In addition to the intrinsic difference in image acquisition for AFM and TEM, it should also be considered that for TEM imaging the sample has to be supported on a carbon film and stained with a heavy-atom salt, to remove the water solution and keep the polymer on the grid once the grid is inserted into the high vacuum environment of the microscope column. To evaluate the possible effect of drying on the sample morphology, two different protocols were applied to minimize artefacts due to sample preparation. In the fast-drying procedure, a drop of a uranyl acetate solution, used as a stain, is immediately added to fix the polymer on the grid. Then, water is quickly removed from the sample by blotting with a filter paper so that the drop is dried within seconds. The slow-drying protocol follows a procedure more similar to the sample preparation for AFM, with the slow removal of the water solution over several hours, followed by stain fixation.

In agreement with the AFM measurements, TEM micrographs show round particles (Fig. 4a-c), with average diameters of 60 ± 12 nm (Supplementary Fig. S3). Samples prepared with the two alternative procedures showed similar results, but for the homogeneity of the particle distribution on the grid. When the fast-drying procedure was applied, particles were more homogeneously dispersed on the grid, while in the slow-drying procedure, particles were concentrated in a few grid squares on the borders of the grid (Fig. 4d). Few particles show straight edges compatible with some internal order (e.g., Fig. 4a–b). In a few cases, particles appear aggregated in pairs or larger groups, with a

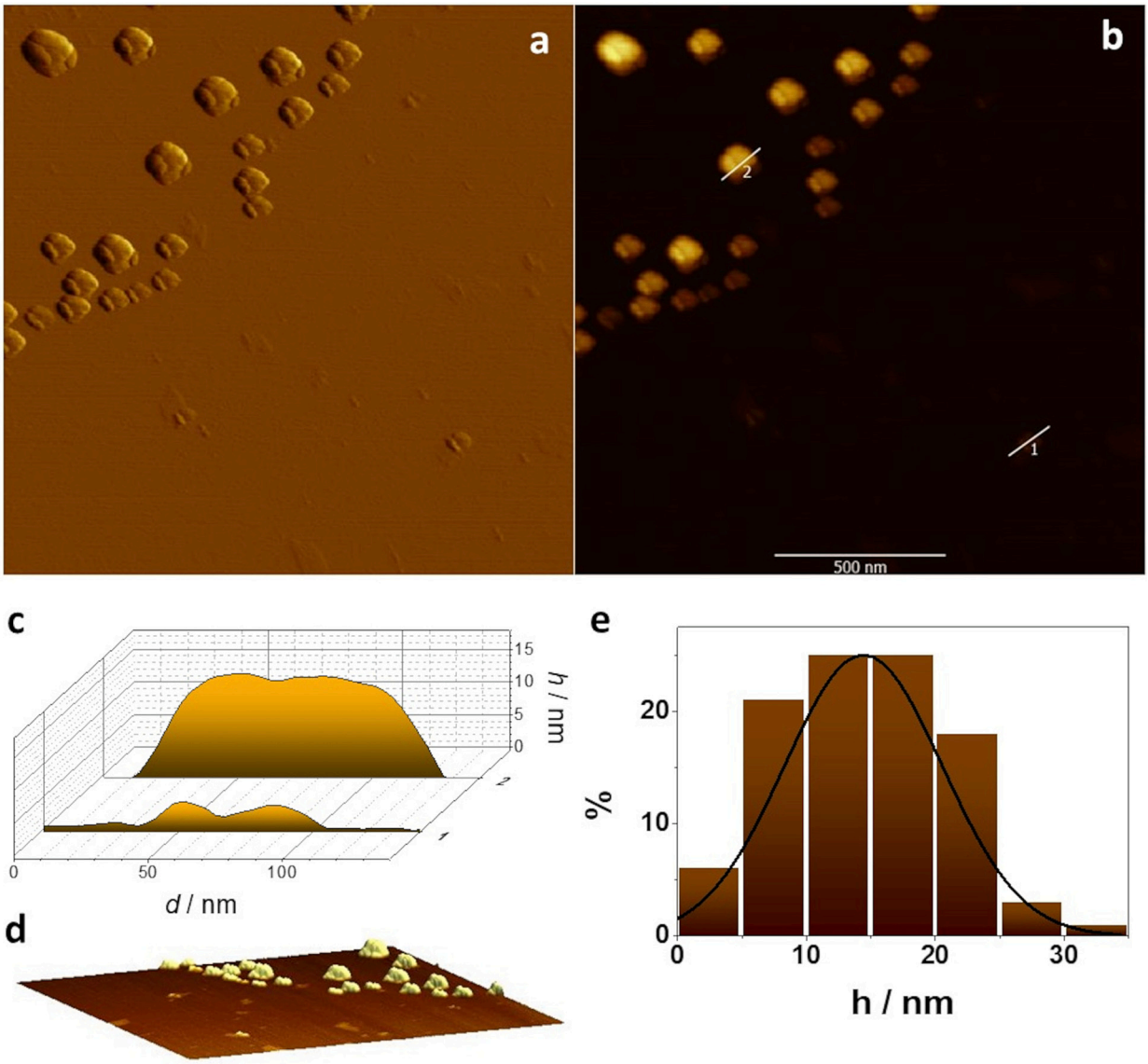

Fig. 2. Dry state AFM images of Epol C1576 obtained from 5 μg/mL solutions. a) polymer chain structures exhibiting a more structured morphology; b) and c) profiling of one of the objects in panel a; d) three-dimensional view of a); e) statistics of the vertical dimension of the objects in panel a).

distinguishable round shape of each particle (Fig. 5), as also indicated by the bimodal shape of the size distribution analysis (Supplementary Fig. S3).

Despite the negative staining protocol used to prepare the samples, particles appear darker than the background. Effects of staining are hard to predict; a survey of the literature shows similar images for other polysaccharides [28] but no explanation is given for the phenomenon.

3.3. Modelling

The computer modelling of the Epol C1576 three-dimensional conformation as it appears from both AFM and TEM images is not an easy task. In fact, quantification from AFM images suggests that the polysaccharide forms multichain aggregates with uncertain stoichiometry. In addition, polymer chains exhibit a molar mass distribution and water molecules might play an important role in defining the three-dimensional architecture. The modelling study was carried out with two aims. Firstly, the flexibility of the polymer backbone was tested to assess its ability to form compact structures, in the absence of solvent (water). Then, the tendency to form compact multichain aggregates was tested in the presence of explicit water.

The modelling in the absence of solvent showed that a polysaccharide segment composed of 34 repeating units and initially configured as a coiled chain, is able to collapse into a compact structure after a 0.5 ns dynamic simulation due to van der Waals attraction forces. This result demonstrates rather high chain flexibility, as reported in Fig. 6, where the gyration radius evolution is also displayed.

The modelling study in the presence of explicit water was more complex. Sixteen polymer segments, each composed of 16 sugar monomers (4 repeating units), were placed into a simulation box in the presence of 4468 water molecules (50 % polysaccharide-to-water mass ratio) and simulated without constraints for a total of 600 ns. The dynamics simulation showed the spontaneous formation of a relatively compact and stable globular aggregate of the 16 chains with an overall gyration radius of around 30 Å, which remained almost constant during the simulation time. The observed aggregate was not static, as chains both escaped and re-joined during this long period but with a strong tendency toward association. The packing within the aggregates was not as dense as, for example, in a folded protein but voids and crevices were filled with water molecules, and thus the aggregates resembled more closely known polysaccharide gels (see Fig. 8).

The evolution of the gyration and hydrodynamic radiuses are shown

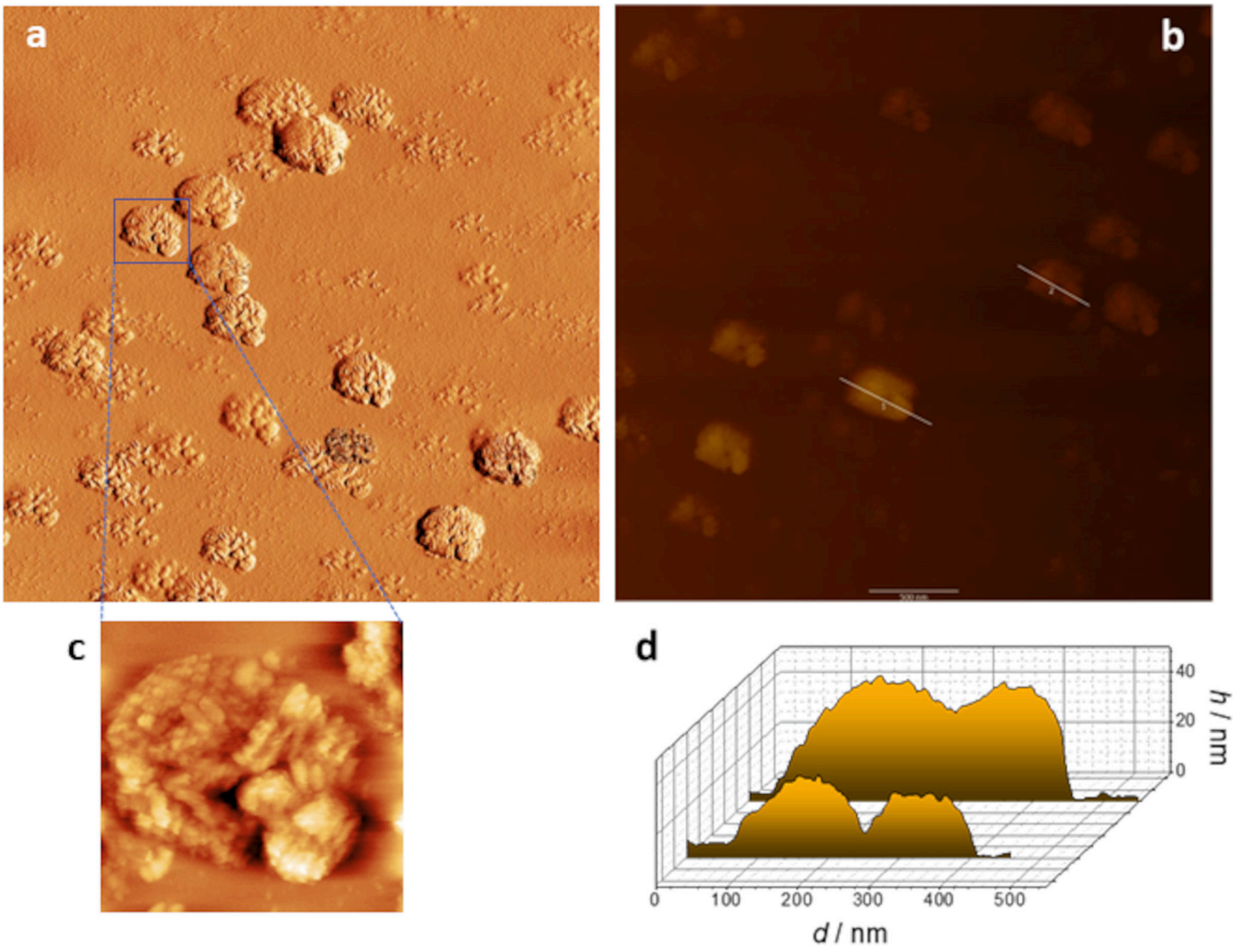

Fig. 3. a) AFM image of Epol C1576 in solution; b) and d) profiling of some detected objects; c) enlargement of one object of panel a.

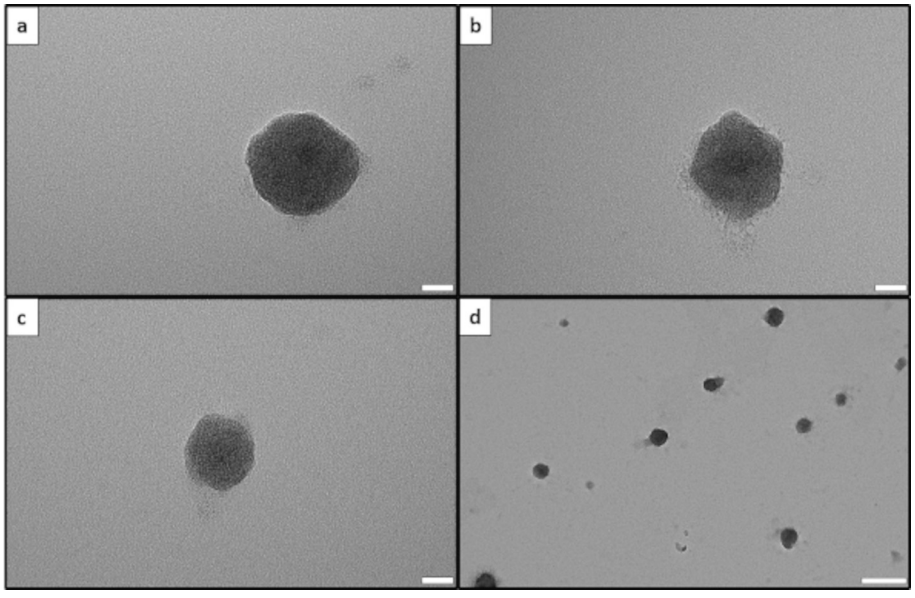

Fig. 4. TEM micrographs of Epol C1576 obtained with the fast-drying (a–c) or slow-drying (d) procedure. Dimension bars correspond to 20 nm for panels (a–c) and to 200 nm for panel (d).

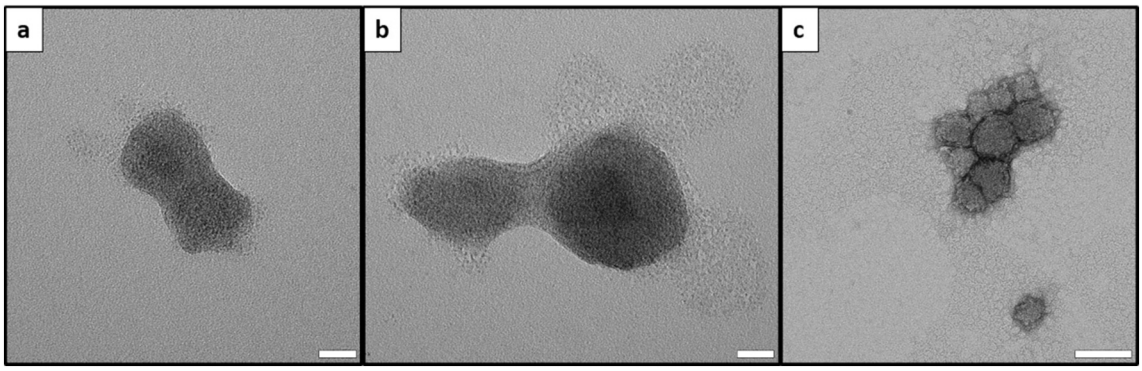

Fig. 5. TEM micrographs of Epol C1576 obtained with the fast-drying (a–b) or slow-drying (c) procedure showing pairs or aggregates of round particles. Dimension bars correspond to 20 nm for panels (a-b) and to 100 nm for panel (c).

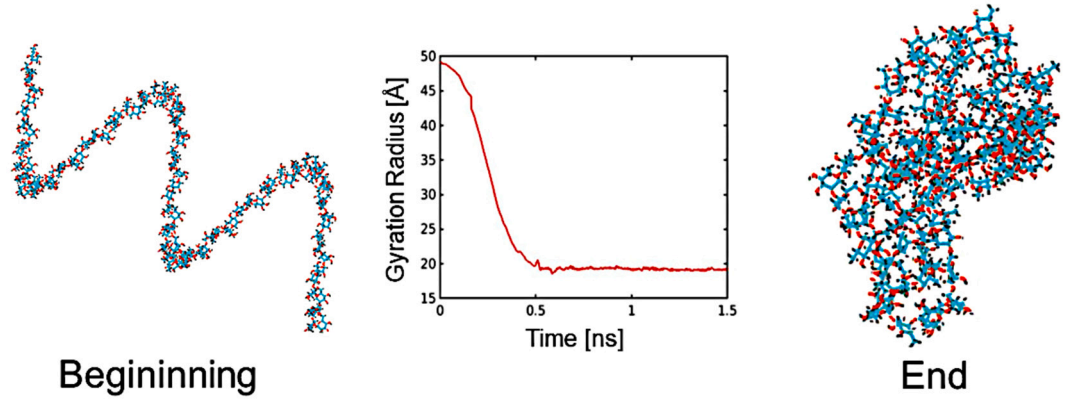

Fig. 6. Snapshot of the Epol C1576 chain at the beginning and at the end of the simulation. The polymer collapsed from its starting randomized relaxed configuration to a tightly packed globular form in 0.5 ns.

in Fig. 7. The increase in the gyration radius of the system of the polysaccharide chains at around 200 ns (Fig. 7) is due to one of the single chain "freeing" itself from the aggregate and moving around before coming back to the large aggregate, thus causing a decrease in the overall gyration radius at around 600 ns. The slight increase after 600 ns is due to another chain moving away from the aggregate and then back to the aggregate soon afterwards. As no permanent chemical bonds are formed between the chains, random movements of some of the polysaccharidic chains are expected from time to time. Representative snapshots of the conformations assumed by the 16 polymeric sequences within the aggregate structure are shown in Fig. 8, (panel a: initial time; panel b: after 600 ns, and panel c: after 800 ns).

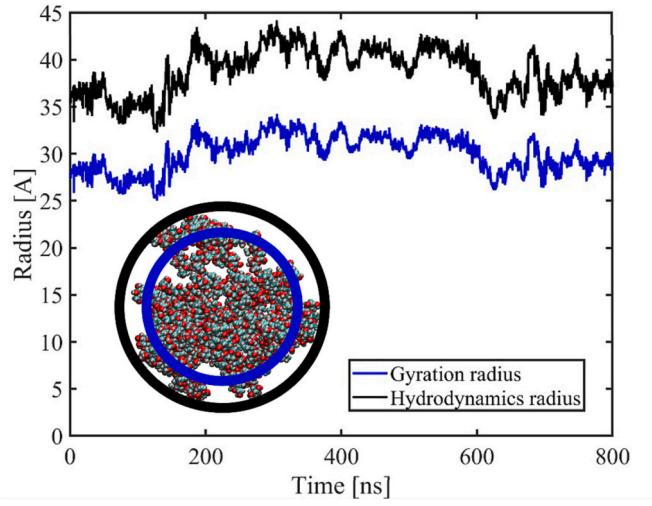

Fig. 7. Hydrodynamic radius of the system of Epol C1576 varies throughout the simulation time. The inset shows a qualitative representation of the polysaccharide system and hydrodynamic radius (black circle) and gyration radius (blue circle).

Considering that the gyration radius is proportional to the total length of a polymer throughout the square root of its persistence length, which defines the extent of chain flexibility, it is possible to speculate about the ratio between the known molecular mass of the modelled system (256 sugar monomers, corresponding to a molecular mass of about 4000 Da) and the unknown molecular mass of a mean object as detected by AFM. The gyration radius of the modelled system is about 3 nm, while the radius quantified from AFM analysis ranges from 20 to 10 nm. The ratio between the two figures is in the range 0.3–0.15 which corresponds to a polymer mass in the range 650–1800 kDa. These values are in good agreement with the molecular mass of Epol C1576, as evaluated by HPSEC analysis which gives an average value of 622 kDa (Supplementary Fig. S4). This qualitative analysis based on the gyration radius data suggests that the smallest objects detected by AFM analysis are composed of a single polymer chain, while the largest contain up to 4 chains.

4. Conclusions

The present study elucidates in depth the possible relationships between the chemical structure, the macromolecular behaviour, and the role that the exopolysaccharide produced by *B. multivorans* C1576 covers in the biofilm matrix architecture. AFM data on both dry samples

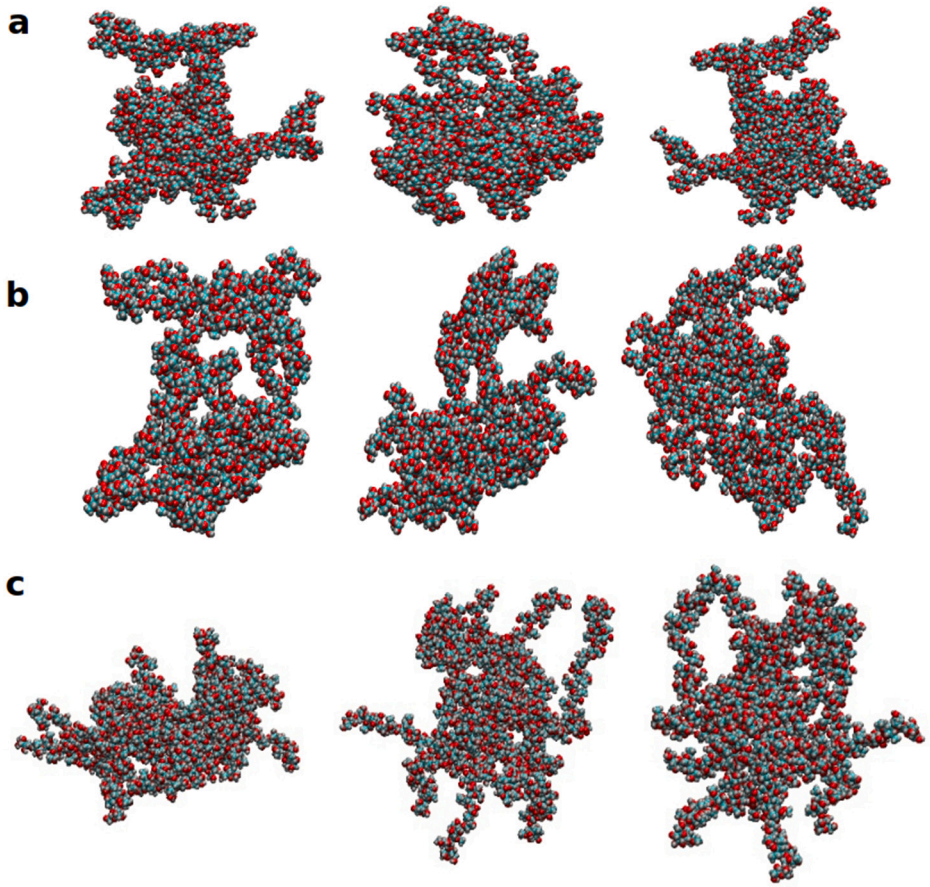

Fig. 8. Different views of the 16 polymer segments system. a) Beginning of the simulation; b) after 600 ns simulation; c) after 800 ns simulation.

and samples dissolved in water clearly show that the polymer can fold into a compact globular structure and EM data confirmed this behaviour. In addition, in more concentrated systems the globules aggregate forming more complex structures. The globules exhibit different dimensions depending on the polydisperse nature of the polysaccharide molecular mass and the possible aggregation of more than one polymer chain into a single globule.

Despite the large simulations carried out for long times, MD results are not sufficiently converged to calculate statistically meaningful thermodynamic association free energies. Nonetheless, they do indicate a clear spontaneous intrinsic aggregation affinity on the part of these chains. Future work with larger boxes containing even more chains, for longer times, and at different concentrations, will be carried out to extract information on the molecular determinants involved in the aggregation, focusing on the role of the rhamnose residues, and particularly on the methylated rhamnose rings.

The ability of polysaccharides to form folded compact structures certainly depends on the polymer chain flexibility, but a relevant role is also played by the presence of rhamnose residues in the polymer repeating unit sequence. These confer a less polar character to the backbone and allow the formation of relevant van der Waals interactions which help both the folded globule formation and interchain aggregation. These aspects are relevant for the biofilm matrix formation since it requires a water-swollen structure that does not allow its components to dissolve in the aqueous environment. In addition, the presence of non-polar patches on globules, and globule aggregates, may favour the retention into the matrix of components with low water solubility, essential for the bacterial collective quorum system as signalling agents.

CRediT authorship contribution statement

Michele Cacioppo: Investigation, Methodology, Writing – original draft. **Rita De Zorzi:** Investigation, Methodology, Writing – original draft. **Zois Syrgiannis:** Investigation, Methodology, Data curation. **Barbara Bellich:** Investigation, Methodology, Visualization. **Paolo Bertoncin:** Methodology, Formal analysis. **Ining A. Jou:** Investigation, Methodology, Visualization. **John W. Brady:** Conceptualization, Supervision, Funding acquisition, Writing – original draft. **Roberto Rizzo:** Conceptualization, Data curation, Writing – original draft. **Paola Cescutti:** Conceptualization, Supervision, Data curation, Writing – review & editing.

Declaration of competing interest

The authors declare that they have no conflicts of interest with the contents of this article.

Acknowledgments

This work was supported by the National Institutes of Health (USA), (Grant Number GM123283).

Appendix A. Supplementary data

Supplementary data to this article can be found online at https://doi.org/10.1016/j.ijbiomac.2023.127294.

References

[1] H.-C. Flemming, J. Wingender, U. Szewzyk, P. Steinberg, S.A. Rice, S. Kjelleberg, Biofilms: an emergent form of bacterial life, Nat. Rev. Microbiol. 14 (2016) 6563–6575, https://doi.org/10.1038/nrmicro.2016.94.

[2] C.A. Fux, J.W. Costerton, P.S. Stewart, P. Stoodley, Survival strategies of infectious biofilms, Trends Microbiol. 13 (2005) 34–40, https://doi.org/10.1016/j.tim.2004.11.010.

[3] L.A. Hawver, S.A. Jung, W.-L. Ng, Specificity and complexity in bacterial quorum-sensing systems, FEMS Microbiol. Rev. 40 (2016) 738–752, https://doi.org/10.1093/femsre/fuw014.

[4] D.G. Allison, The biofilm matrix, Biofouling 19 (2003) 139–150, https://doi.org/10.1080/0892701031000072190.

[5] S.S. Branda, Å. Vik, L. Friedman, R. Kolter, Biofilm: the matrix revisited, Trends in Microbiol. 13 (2005) 20–26, https://doi.org/10.1016/j.tim.2004.11.006.

[6] D.H. Limoli, C.J. Jones, D.J. Wozniak, Bacterial extracellular polysaccharides in biofilm formation and function, Microbiol. Spectr. Jun;3 (3) (2015), https://doi.org/10.1128/microbiolspec.MB-0011-2014.

[7] B. Cuzzi, Y. Herasimenka, A. Silipo, R. Lanzetta, G. Liut, R. Rizzo, P. Cescutti, Versatility of the *Burkholderia cepacia* Complex for the biosynthesis of exopolysaccharides: a comparative structural investigation, PloS One 9 (2014), e94372, https://doi.org/10.1371/journal.pone.0094372.

[8] M.J. Franklin, D.E. Nivens, J.T. Weadge, P.L. Howell, Biosynthesis of the *Pseudomonas aeruginosa* extracellular polysaccharides, alginate, Pel, and Psl, Front. Microbiol. 2 (167) (2011) 1–10, https://doi.org/10.3389/fmicb.2011.00167.

[9] B. Bellich, I.A. Jou, C. Buriola, N. Ravenscroft, J.W. Brady, M. Fazli, T. Tolker-Nielsen, R. Rizzo, P. Cescutti, The biofilm of *Burkholderia cenocepacia* H111 contains an exopolysaccharide composed of rhamnose and L-mannose: structural characterization and molecular modelling, Carbohydr. Res. 499 (2021) 108231, https://doi.org/10.1016/j.carres.2020.108231.

[10] B. Bellich, I.A. Jou, M. Caterino, R. Rizzo, N. Ravenscroft, M. Fazli, T. Tolker-Nielsen, J.W. Brady, P. Cescutti, *Burkholderia cenocepacia* H111 produces a water-insoluble exopolysaccharide in biofilm: Structural dDetermination and molecular modelling, Int. J. Mol. Sci. 21 (2020) 1702–1714, https://doi.org/10.3390/ijms21051702.

[11] P. Vandamme, P. Dawyndt, Classification and identification of the *Burkholderia cepacia* complex: past, present and future, Syst. Appl. Microbiol. 34 (2011) 87–95, https://doi.org/10.1016/j.syapm.2010.10.002.

[12] E. Vanlaere, A. Baldwin, D. Gevers, D. Henry, E. De Brandt, J.J. LiPuma, E. Mahenthiralingam, D.E. Speert, C. Dowson, P. Vandammeet, K. Taxon, A complex within the *Burkholderia cepacia* complex, comprises at least two novel species, *Burkholderia contaminans* sp. nov. and *Burkholderia lata* sp. nov, Int. J. Syst. Evol. Microbiol. 59 (2009) 102–111, https://doi.org/10.1099/ijs.0.001123-0. PMID: 19126732.

[13] B. De Smet, M. Mayo, C. Peeters, J.E. Zlosnik, T. Spilker, T.J. Hird, J.J. LiPuma, T. J. Kidd, M. Kaestli, J.L. Ginther, D.M. Wagner, P.S. Keim, S. Bell, J.A. Jacobs, B. Currie, P. Vandamme, et al., *Burkholderia stagnalis* sp. nov. and *Burkholderia territorii* sp. nov.; two novel *Burkholderia cepacia* complex species from environmental and human sources, Int. J. Syst. Evol. Microbiol. 65 (2015) 2265–2271, https://doi.org/10.1099/ijs.0.000251.

[14] P. Martina, M. Leguizamon, C.I. Prieto, S.A. Sousa, P. Montanaro, W.O. Draghi, M. Stämmler, M. Bettiol, C.C. de Carvalho, J. Palau, C. Figoli, F. Alvarez, S. Benetti, S. Lejona, C. Vescina, J. Ferreras, P. Lasch, A. Lagares, A. Zorreguieta, J.H. Leitão, O.M. Yantorno, A. Bosch, *Burkholderia puraquae* sp. nov., a novel species of the *Burkholderia cepacia* complex isolated from hospital settings and agricultural soils, Int. J. Syst. Evol. Microbiol. 68 (2018) 14–20, https://doi.org/10.1099/ijsem.0.002293.

[15] K. De Boeck, A. Malfroot, L. Van Schil, P. Lebecque, C. Knoop, J.R.W. Govan, C. Doherty, S. Laevens, P. Vandamme, L. Van Schil, J.P. Ursi, K. Desager, G. Ieven, A. Mertens, I. Dab, S. Lauwers, J. Gigi, M. Struelens, H. Franckx, F. De Baets, S. Vandaele, G. Verschraegen, M. Proesmans, J. Van Eldere, F. Lebrun, F. Pauquay, E. Bodart, Y. Glupczynski, C. Sevens, Epidemiology of *Burkholderia cepacia* complex colonisation in cystic fibrosis patients, Eur. Respir. J. 23 (2004) 851–856, https://doi.org/10.1183/09031936.04.00118804.

[16] S. Dolfi, A. Sveronis, A. Silipo, R. Rizzo, P. Cescutti, A novel rhamno-mannan exopolysaccharide isolated from biofilms of *Burkholderia multivorans* C1576, Carbohydr. Res. 411 (2015) 42–48, https://doi.org/10.1016/j.carres.2015.04.012.

[17] M.M. Kuttel, P. Cescutti, M. Distefano, R. Rizzo, Fluorescence and NMR spectroscopy together with molecular simulations reveal amphiphilic characteristics of a *Burkholderia* biofilm exopolysaccharide, J. Biol. Chem. 292 (2017) 11034–11042, https://doi.org/10.1074/jbc.M117.785048.

[18] B. Bellich, M. Distefano, Z. Syrgiannis, S. Bosi, F. Guida, R. Rizzo, J.W. Brady, P. Cescutti, The polysaccharide extracted from the biofilm of *Burkholderia multivorans* strain C1576 binds hydrophobic species and exhibits a compact 3D-structure, Int. J. Biol. Macromol. 136 (2019) 944–950, https://doi.org/10.1016/j.ijbiomac.2019.06.140.

[19] E. Mahenthiralingam, T. Coenye, J.W. Chung, D.P. Speert, J.R.W. Govan, P. Taylor, P. Vandamme, Diagnostically and experimentally useful panel of strains from the *Burkholderia cepacia* Complex, J. Clin. Microbiol. 38 (2000) 910–913, https://doi.org/10.1128/JCM.38.2.910-913.2000.

[20] B.R. Brooks, R.E. Bruccoleri, B.D. Olafson, S. Swaminathan, M. Karplus, CHARMM: a program for macromolecular energy, minimization, and dynamics calculations, J. Comput. Chem. 4 (1983) 187–217, https://doi.org/10.1002/jcc.540040211.

[21] B.R. Brooks, C.L. Brooks III, A.D. Mackerell Jr., L. Nilsson, R.J. Petrella, B. Roux, Y. Won, G. Archontis, C. Bartels, S. Boresch, A. Caflisch, L. Caves, Q. Cui, A. R. Dinner, M. Feig, S. Fischer, J. Gao, M. Hodoscek, W. Im, K. Kuczera, T. Lazaridis, J. Ma, V. Ovchinnikov, E. Paci, R.W. Pastor, C.B. Post, J.Z. Pu, M. Schaefer, B. Tidor, R.M. Venable, H.L. Woodcock, X. Wu, W. Yang, D.M. York, M. Karplus, CHARMM: the biomolecular simulation program, J. Comput. Chem. 30 (2009) 1545–1614, https://doi.org/10.1002/jcc.21287.

[22] I.A. Jou, M. Caterino, U. Schnupf, R. Rizzo, P. Cescutti, J.W. Brady, Ramachandran conformational energy maps for disaccharide linkages found in *Burkholderia multivorans* biofilm polysaccharides, Int. J. Biol. Macromol. 143 (2020) 501–509, https://doi.org/10.1016/j.ijbiomac.2019.11.037.

[23] I.A. Jou, A.S. Yoo, E.V. Dionne, J.W. Brady, Potential of mean force conformational energy maps for disaccharide linkages of the *Burkholderia multivorans* exopolysaccharide C1576 in aqueous solution, Carbohydr. Res. 524 (2023) 108741, https://doi.org/10.1016/j.carres.2023.108741.

[24] W.L. Jorgensen, J. Chandrasekhar, J.D. Madura, R.W. Impey, M.L. Klein, Comparison of simple potential functions for simulating liquid water, J. Chem. Phys. 79 (1983) 926–935, https://doi.org/10.1063/1.445869.

[25] P. Mark, L. Nilsson, Structure and dynamics of the TIP3P, SPC, and SPC/E water models at 298 K, J. Phys. Chem. A 105 (2001) 9954–9960, https://doi.org/10.1021/jp003020w.

[26] D.A. Case, K. Belfon, I.Y. Ben-Shalom, S.R. Brozell, D.S. Cerutti, T.E. Cheatham III, V.W.D. Cruzeiro, T.A. Darden, R.E. Duke, G. Giambasu, M.K. Gilson, H. Gohlke, A. W. Goetz, R. Harris, S. Izadi, S.A. Izmailov, K. Kasavajhala, A. Kovalenko, R. Krasny, T. Kurtzman, T.S. Lee, S. LeGrand, P. Li, C. Lin, J. Liu, T. Luchko, R. Luo, V. Man, K.M. Merz, Y. Miao, O. Mikhailovskii, G. Monard, H. Nguyen, A. Onufriev, F. Pan, S. Pantano, R. Qi, D.R. Roe, A. Roitberg, C. Sagui, S. Schott-Verdugo, J. Shen, C.L. Simmerling, N.R. Skrynnikov, J. Smith, J. Swails, R.C. Walker, J. Wang, L. Wilson, R.M. Wolf, X. Wu, Y. Xiong, Y. Xue, D.M. York, P.A. Kollman, AMBER 2020, University of California, San Francisco, 2020.

[27] T.C. John Towns, M. Dahan, I. Foster, K. Gaither, A. Grimshaw, V. Hazlewood, S. Lathrop, D. Lifka, G.D. Peterson, R. Roskies, J.R. Scott, N. Wilkins-Diehr, XSEDE: accelerating scientific discovery, Comput. Sci. Eng. 16 (2014) 62–74, https://doi.org/10.1109/MCSE.2014.80.

[28] J.L. Putaux, A. Buléon, R. Borsali, H. Chanzy, Ultrastructural aspects of phytoglycogen from cryo-transmission electron microscopy and quasi-elastic light scattering data, Int. J. Biol. Macromol. 26 (1999) 145–150, https://doi.org/10.1016/s0141-8130(99)00076-8.